ISBN: 978-3-95450-214-1 ISSN: 2673-5490 doi:10.18429/JACoW-IPAC2021-THXC06

DESIGN AND MEASUREMENTS OF AN X-BAND 8 MeV STANDING-WAVE ELECTRON ACCELERATOR*

Focheng Liu[1], Jiaru Shi[1], Hao Zha[†1], Huaibi Chen[1], Chuanxiang Tang[1]
Department of Engineering Physics, Tsinghua University, Beijing, China
[1]also at Key Laboratory of Particle and Radiation Imaging of Ministry of Education, Tsinghua University, Beijing, China

Abstract

X-band low-energy electron linear accelerators are attractive to industrial and medical applications due to the compact size. This work we present design and tests of an 8 MeV X-band accelerator for industrial use. It adopts the coaxial coupling standing wave structure working at 9300 MHz. The accelerator length is 48 cm including the cavity, thermal gun and the electron window. Dedicated bunching cells are designed to reduce the energy spread. In the high power tests, the accelerator was able to generated the electron beam with RMS energy spread 1.1% (beam energy: 8.1 MeV, peak current: 45 mA). Combining features of compact size and the low energy spread, this X-band accelerator design is valuable for various application.

INTRODUCTION

Low-energy electron linear accelerators are widely used in industrial and medical applications [1-6], such as radiotherapy, non-destructive testing, processing irradiation, sterilization, and so on.

X-band accelerators show promising application prospects, because of compactness and high accelerating efficiency. Besides, X-band accelerators contribute to less energy spread, compared to lower frequency bands.

Large energy spread causes beams' maximum energy increasing and average energy decreasing. Furthermore, electron penetration depth is reduced, which results in more surface dose deposition for electron radiotherapy and more heat deposition in X-ray converters for X-ray radiotherapy, due to large energy spread. X-ray dose rate is also reduced. What's more, significant dispersion happens to beams with large energy spread in a magnetic system and causes large penumbra areas, which would reduce the efficiency of industrial irradiation and sterilization accelerators. Compared to lower frequency bands, X-band accelerators have more cell number in same length, more freedom to optimize the length and the electronic field of bunching cells, and less charge in one periodic bunch with similar transverse size causing less space charge effect, so the better energy spread performance can be achieved.

This work presents an X-band 8 MeV standing-wave electron accelerator. The accelerator length is 48 cm including the cavity, thermal gun and the electron window. Dedicated bunching cells are designed to reduce the energy spread. In the high power tests, the accelerator was able to generated the electron beam with RMS energy spread 1.1%, which is comparable to photocathode RF guns for research application. Combining features of compact size and the low energy spread, this X-band accelerator design is valuable for various application.

DESIGN

Lattice Design

A good performance of RF bunching without solenoids is achieved by cavity optimization. As shown in Fig. 1, the beam transverse envelope size increases slightly in the first few cells and then decreases in next accelerating cells, and the performances on X and Y axis are similar. Triple the rms value of beam transverse envelope size doesn't exceed the radius of beam aperture 1.75 mm. The energy of beams increases slowly in bunching cells and increases rapidly with a linear slope.

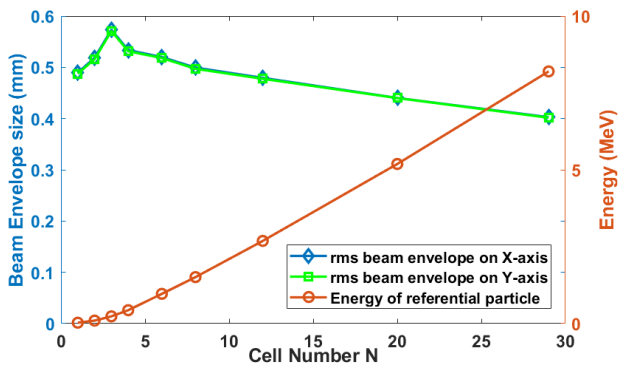

Figure 1: Rms value of transverse beam envelope size on X-axis (blue) and Y-axis (green), and the energy of referential particle (red) versus the cell number.

Figure 2 shows the longitudinal phase spaces of electron beams at different cells, which demonstrate the longitudinal bunching process. The horizontal and vertical axis are phase and normalized energy of beams, respectively. The values of colormap are not normalized to the maximum among all figures, because all dots except few points turn into blue with normalization and the process of longitudinal bunching becomes obvious. The emitted beams are uniform on the phase, because of the thermal DC gun. Significant longitudinal bunching effect is displayed in Fig. 2. The most of beams collect together in the phase space, with a blue tail shown in the figure.

* Work supported by The National Key Research and Development Program of China (Grand No: 2017YFC0111700)
† zha_hao@mail.tsinghua.edu.cn

ISBN: 978-3-95450-214-1 ISSN: 2673-5490 doi:10.18429/JACoW-IPAC2021-THXC06

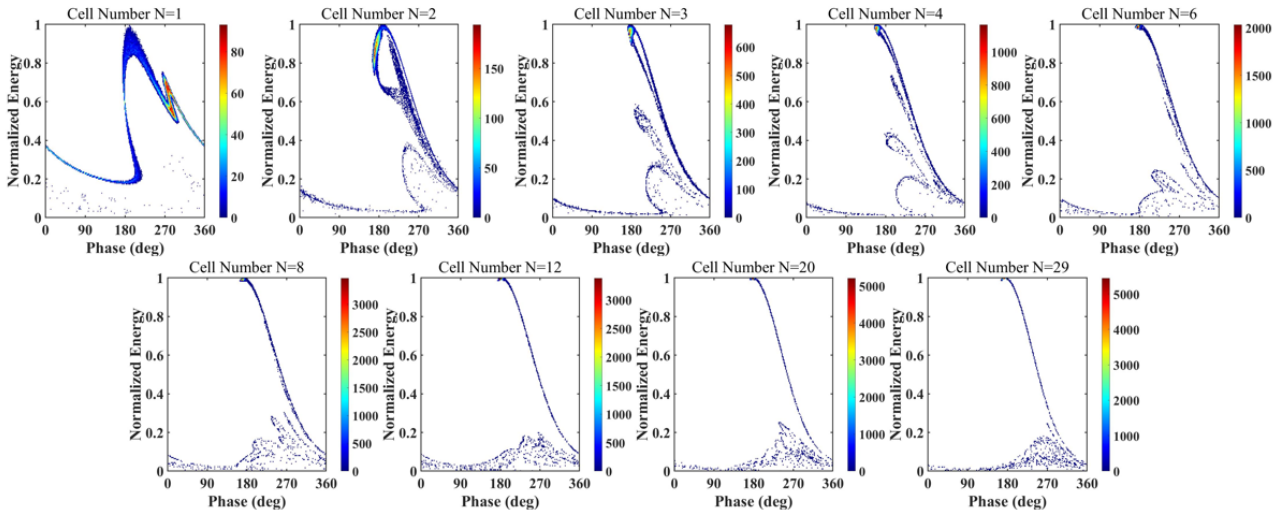

Figure 2: Longitudinal phase spaces of electron beams at different cells.

Figure 3 is energy spectrums with different input powers. With 1.77 MW power input, the energy of the conferential particle is 8.19 MeV. A low energy spread with thermal DC electron gun is achieved without solenoids. The FWHM value of energy spread is 0.04 MeV (0.5%) and the rms value is 0.09 MeV (1.1%), which is even comparable to the energy spread of photocathode RF guns with solenoids for research applications. Figure 3 also shows a certain capability of energy adjustment. Even the energy spread with 1.96 MW power input is 5%, better than some industrial accelerators without optimization of energy spread.

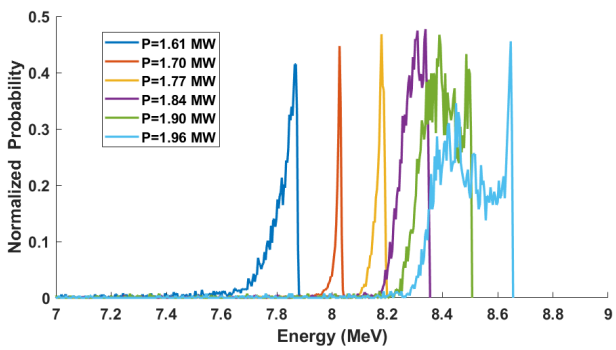

Figure 3: Energy spectrums with different input powers.

RF Design

The RF simulation is completed in CST. Figure 4 (a) is the electric distribution of accelerator model. The accelerator is designed at $\pi/2$ mode and has 29 accelerating cells and 28 coupling cells with biperiodic structure. The length and maximum accelerating electric field of bunching cells are optimized to less values than accelerating cells for a better performance of RF bunching. Figure 4 (b) is the dispersion curve of the accelerator. The horizontal is frequency and vertical axis is reflection S parameter S_{11}. Every single peak represents a working mode and the highest one is the $\pi/2$ mode. The working frequency of $\pi/2$ mode is 9300 MHz and the frequency space is 18 MHz, which guarantees a good mode stability in practice.

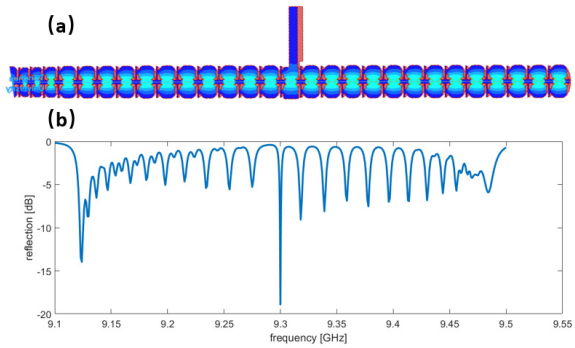

Figure 4: (a) The electric distribution of accelerator model and (b) the dispersion curve of the accelerator.

Mechanical Design

The accelerator is machined in 29*2 disks. With a simple numerical estimation, 2 MHz rms frequency shift would result in 0.5% reduction in accelerating voltage, which is acceptable. Thus, tuning pins are removed, reducing the cost significantly and making practical application much easier. The frequency error among processed accelerating cells is below 2 MHz. The large frequency error of few individual cells can be tuned by controlling cell radius. The disks are brazed by silver-based alloys, and no significant frequency shift is observed after brazing. Figure 5 is the picture of the X-band accelerator after brazing. Design parameters of accelerator is in Table 1.

Figure 5: Picture of the X-band accelerator after brazing.

ISBN: 978-3-95450-214-1 ISSN: 2673-5490 doi:10.18429/JACoW-IPAC2021-THXC06

Table 1: Design Parameter Table of X-Band Accelerator

Parameter	Value
Working frequency	9300 MHz
Working mode	π/2 biperiodic mode
Cell amount	29 accelerating cells + 28 coupling cells
Whole length	44.2 cm (cells) + 3.8 cm (gun)
Input power	1.8 MW
Peak current	45 mA
Beam energy	8.1 MeV
Energy spread FWHM	0.04 MeV (0.5%)
RF pulse length	4 us
Repetition rate	5-250 Hz

ENERGY SPECTRUM MEASUREMENT

Measurement Result

Figure 6 (a) is the schematic diagram of experiment layout, and Fig. 6 (b) is the picture of the experiment set-up. Electron beams go through a titanium window after accelerating. The collimator is to limit the position and direction of beams. By the magnetic field in the magnetic analyzer, the dispersion effect makes beams with different energy reach and image at the different position on a YAG screen. The images are reflected by a mirror away from the beamline and recorded by a camera.

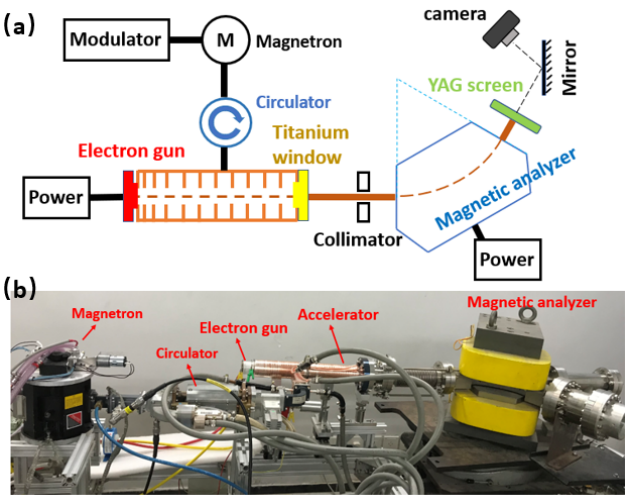

Figure 6: (a) The schematic diagram of experiment layout and (b) the picture of the experiment set-up.

Figure 7 is the measured energy spectrums with different input power. Among these four input powers, the minimum FWHM energy spread is 0.15 MeV with 1.79 MW power input. Compared to the simulation results, energy spreads are larger and high energy section is broadening.

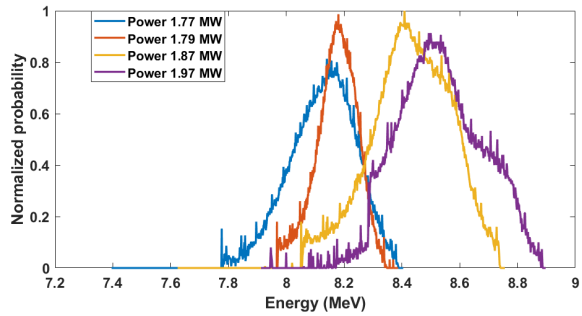

Figure 7: The measured energy spectrums with different input power.

Real-time Analysis of Power Fluctuating

Power fluctuating effect is normal in pulsed low-energy accelerators because of the beam loading and the wave form of pulsed power. The field in accelerator with beams E(t) consists of two parts, RF field without beams A(t) and the field caused by beam loading B(t), which is expressed in Eq. (1).

$$E(t) = A(t) + B(t). \quad (1)$$

A(t) is related to the input power P(t). B(t) is covariant with beam current $I_b(t)$, while $I_b(t)$ is related to the bunching effect of the total field E(t). With the input power and the thermal electron gun current pulse form as the initial condition in the iterative calculation process, the bunch current is simulated and agrees well with the measured data. Further, the power fluctuating effect in bunching process can be quantitatively analysed, and the modified result is closer to the measured result, shown in Fig. 8.

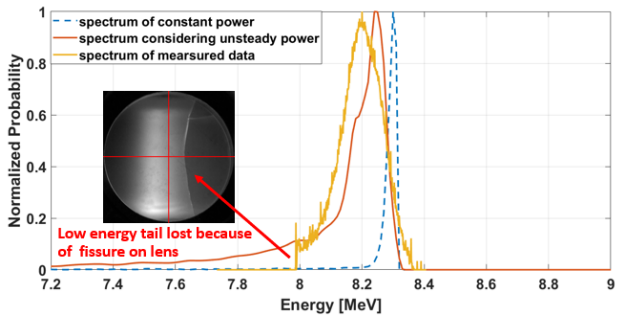

Figure 8: The modified result of power fluctuating.

The energy spectrum measurement is affected by other factors, such as emittance and energy spread growth by scattering with titanium window, and system resolution ratio related to the transverse phase space. These factors can be restrained by the collimator while extra particles are lost. In the data analysis, the main factor is power fluctuating at the experiment set-up in our laboratory.

CONCLUSION

This work presents an X-band 8 MeV standing-wave electron accelerator. Combining features of compact size and the low energy spread, this X-band accelerator design is valuable for various application.

ISBN: 978-3-95450-214-1 ISSN: 2673-5490 doi:10.18429/JACoW-IPAC2021-THXC06

REFERENCES

[1] S. M. Hanna, "Applications of X-Band Technology in Medical Accelerators", in *Proc. 18th Particle Accelerator Conf. (PAC'99)*, New York, NY, USA, Mar. 1999, paper WEP114, pp. 2516-2518.

[2] A. V. Mishin, "Advances in X-Band and S-Band Linear Accelerators for Security, NDT, and Other Applications", in *Proc. 21st Particle Accelerator Conf. (PAC'05)*, Knoxville, TN, USA, May 2005, paper FOAB002, pp. 240-244.

[3] B. N. Lee *et al.*, "Status of KAERI 6 MeV 9.3 GHz X-Band Electron Linac for Cancer Treatment System", in *Proc. 5th Int. Particle Accelerator Conf. (IPAC'14)*, Dresden, Germany, Jun. 2014, pp. 2168-2170. doi:10.18429/JACoW-IPAC2014-WEPRO090

[4] C. F. Eckman, T. Downer, A. Andrews, P. Buaphad, and Y. Kim, "Design of a Compact X-Band Linac Structure for KAERI-RTX-ISU Medical Cyberknife Project", in *Proc. North American Particle Accelerator Conf. (NAPAC'13)*, Pasadena, CA, USA, Sep.-Oct. 2013, paper THPSM16, pp. 1418-1420.

[5] Yuzheng Lin, "Applications of Low Energy Linacs in China", in *Proc. 21st Linear Accelerator Conf. (LINAC'02)*, Gyeongju, Korea, Aug. 2002, paper TU203, pp. 279-283.

[6] S. M. Hanna, "Review of Energy Variation Approaches in Medical Accelerators", in *Proc. 11th European Particle Accelerator Conf. (EPAC'08)*, Genoa, Italy, Jun. 2008, paper TUPP117, pp. 1797-1799.